Research Paper

Crucial role of chelatable iron in silver nanoparticles induced DNA damage and cytotoxicity

Agnieszka Grzelak[a], Maria Wojewódzka[b], Sylwia Meczynska-Wielgosz[b], Mariusz Zuberek[a], Dominika Wojciechowska[a], Marcin Kruszewski[b,c,d,*]

[a] Department of Molecular Biophysics, Faculty of Biology and Environmental Protection, University of Lodz, Banacha 12/16, 90-237 Lodz, Poland
[b] Centre for Radiobiology and Biological Dosimetry, Institute of Nuclear Chemistry and Technology, Dorodna 16, 03-195 Warsaw, Poland
[c] Department of Molecular Biology and Translational Research, Institute of Rural Health, Jaczewskiego 2, 20-090 Lublin, Poland
[d] Faculty of Medicine, University of Information Technology and Management, ul. Sucharskiego 2, Rzeszów 35-225, Poland

ARTICLE INFO

ABSTRACT

Damage to mitochondria and subsequent ROS leakage is a commonly accepted mechanism of nanoparticle toxicity. However, malfunction of mitochondria results in generation of superoxide anion radical ($O_2^{\bullet-}$), which due to the relatively low chemical reactivity is rather unlikely to cause harmful effects triggered by nanoparticles. We show that treatment of HepG2 cells with silver nanoparticles (AgNPs) resulted in generation of H_2O_2 instead of $O_2^{\bullet-}$, as measured by ROS specific mitochondrial probes. Moreover, addition of a selective iron chelator diminished AgNPs toxicity. Altogether these results suggest that $O_2^{\bullet-}$ generated during NPs induced mitochondrial collapse is rapidly dismutated to H_2O_2, which in the presence of iron ions undergoes a Fenton reaction to produce an extremely reactive hydroxyl radical ($^{\bullet}OH$). Clarification of the mechanism of NPs-dependent generation of $^{\bullet}OH$ and demonstration of the crucial role of iron ions in NPs toxicity will facilitate our understanding of NPs toxicity and the design of safe nanomaterials.

1. Introduction

Iron is an essential component of many enzymes involved in a variety of biological processes, including electron transfer, oxygen transport, DNA synthesis and repair [1]. Despite its necessity for almost all living organisms, iron in excess is dangerous. In the presence of ferrous ions, hydrogen peroxide undergoes the Fenton reaction to produce an extremely reactive hydroxyl radical ($^{\bullet}OH$). Radical reactions initiated by $^{\bullet}OH$ may result in damage to the macromolecules, such as DNA, lipids and proteins [2,3]. Iron overload has been linked to increased risk of coronary heart disease, inflammation, neurodegenerative disease and cancer [4,5]. Iron content was also reported to correlate with the amount of oxidative damage to DNA [6,7] and with urinary excretion of 8-hydroxy-2-deoxyguanosine [8].

Iron uptake and storage are carried out by different proteins, thus there is a pool of chelatable iron ions (chelatable iron pool, CIP) that reflects a junction of metabolic pathways of iron-containing molecules. Although the CIP represents only a minor fraction of total cellular iron (3–5%), it is easily accessible and engaged in formation of reactive oxygen species (ROS) [9]. Increased ROS production leads to an imbalance between generation of free radicals and their neutralisation by cellular antioxidative defence mechanisms and causes disturbance of the redox equilibrium, known as oxidative stress. Being highly reactive, ROS are able to modify cellular components, causing cyto- and genotoxic effects.

An increase in ROS due to nanoparticles (NPs) treatment is well documented. It has been shown to be a key factor in the biological effects of NPs, both in vivo and in vitro [10–13]. Although low concentrations of ROS are generated during cell respiration under normal physiological conditions, the presence of NPs markedly increases ROS formation, likely due to the interference with mitochondrial or nonmitochondrial ROS producing enzymes. Indeed, an NPs-dependent increase in production of superoxide anion radical ($O_2^{\bullet-}$) by NADPH oxidase, accompanied by intracellular production of the other ROS was recently reported for AgNPs [14] and ultrafine particles [15]. It was also shown that different non-metal NPs co-localize with mitochondrial markers [16]. Also AgNPs of varying size and shape accumulate in the mitochondria [17]. Thus, it seems plausible to assume that AgNPs accumulation could be a direct cause of mitochondrial damage and malfunction of the respiratory chain resulting in ROS generation. For

example, in BRL 3A rat liver cells exposed to AgNPs (15 and 100 nm) the cellular level of ROS increased in a AgNPs concentration-dependent manner and reached a maximum after 6 h [18]. Moreover, in three human cell lines treated with AgNPs, the extent of ROS production correlated with intracellular nanoparticle accumulation and genotoxicity, and negatively with long term cell survival [19]. The recent critical review on AgNPs toxicity leaves no doubts that ROS induction due to the malfunction of mitochondria might be a major cause of detrimental effects exerted by AgNPs on living cells [20].

Here we investigate the mechanism of AgNPs toxicity with special attention paid to generation of ROS and the role of iron in the formation of NPs-induced oxidative damage to DNA and toxicity.

2. Materials and methods

2.1. Chemicals and cell culture

All chemicals, cell culture media ingredients, etc. were purchased from Sigma-Aldrich (Poland) unless otherwise indicated. HepG2 cells were obtained from ATCC. Cells were cultured in cell culture flask with 75 cm^2 surface area (Nunc) in Williams' medium with 10% Fetal Bovine Serum at 37 °C in a 95% moist atmosphere with 5% carbon dioxide. Cells were repassaged when cultures reached 70–85% confluence. Cells were trypsynized, counted using a Countess Automated Cell Counter (Invitrogen) and plated at 4×10^4 per cm^2 new flask or used for experiments.

Depending on the exposure scenario cells were treated simultaneously with 25 µM deferoxamine (DFO) and AgNPs (50 or 100 µg/mL) for 2 h at 37 °C or pre-treated for 24 h with 25 µM DFO and then treated with AgNPs (50 and/or 100 µg/mL) for 2 h at 37 °C. After treatment AgNPs were washed out and cells were left for cytotoxicity assay. For comet assay experiments cells were pretreated for 2 h at 37 °C with DFO at concentration 100 µM to assure substantial removal of CIP and then treated with 10 µg/mL AgNPs for additional 2 h. After treatment cells were immediately processed for DNA damage estimation with the comet assay.

Since combination index approach described by Chuo et al. (for details see [21]) needs a different experimental design, to prevent cytotoxicity resulting from iron deprivation, DFO was used at low-toxic concentration and mixed with AgNPs at a fixed ratio of 1:10. Cells were treated with geometrically increasing concentrations of the mixture. Actual drugs concentrations are presented in CompuSync Report file AgNPs + DFO-d 2.pdf (Supplementary materials). After treatment nanoparticles were washed out and cells were left for cytotoxicity assay.

2.2. Nanoparticle preparation and characterization

AgNPs of nominal size 20 nm were purchased from Plasmachem GmbH, Germany. The stock solution (2 mg/mL) was prepared by suspending of 2 mg AgNPs in 800 µL of distilled water, followed by sonification (4.2 kJ/cm^3, Bronson, USA). Immediately after sonification 100 µL of 15% BSA and 100 µL of a $10 \times$ concentrated phosphate buffered saline [22]. Size and ξ-potential of AgNPs aggregates in suspension were determined by the dynamic light scattering (DLS) method (Zatasier S, Malvern Instruments, Malvern, United Kingdom).

2.3. Neutral Red assay

The Neutral Red (NR) assay was used to assess proliferation of HepG2 cells after treatment with AgNPs, DFO or their combination. The assay was performed as described in [22]. In brief, HepG2 cells were seeded in 96-well microplates (TPP, Switzerland) at a density of 1×10^4 cells/well in 100 µL of culture medium. Twenty four hours after cell seeding, cells were treated as described above. After treatment cell culture medium was removed, the cells were washed with 150 µL PBS and incubated for 3 h at 37 °C with 100 µL of neutral red solution at a

final concentration of 50 µg/mL. Next the NR solution was aspirated, cells were washed with 150 µL of PBS and 200 µL of an acetic acid-ethanol solution (49% water, 50% ethanol and 1% acetic acid) was added to each well. After 15 min of gentle shaking, optical density was read at 540 nm in plate reader spectrophotometer Infinite M200 (Tecan, Austria). At least three independent experiments in six replicate wells were conducted per experimental point.

2.4. Alkaline comet assay

The comet assay (single cell gel electrophoresis) was performed as described in [23]. Briefly, an aliquot of cell suspension was mixed with an equal volume of 2% low melting point agarose (Type VII, Sigma), put on a microscope slide pre-coated with 0.5% normal agarose (Type I-A, Sigma) and left on ice. After agarose solidification, the slides were immersed in ice-cold-lysis solution (2.5 M NaCl, 100 mM Na$_2$EDTA, 10 mM Tris and 1% Triton X-100, pH 10). After 1 h lysis, the slides were placed on a horizontal gel electrophoresis unit filled with a fresh electrophoretic buffer (1 mM Na$_2$EDTA (sodium ethylenediamine tetraacetate) and 300 mM NaOH) and allowed to stay in the buffer for 40 min for DNA unwinding. Next, electrophoresis was performed (1.2 V/cm, 30 min, 10 °C). After electrophoresis, the slides were washed with 0.4 M Tris, pH 7.5 (3 × 5 min) and stained with DAPI (4′,6-diamidino-2-phenylindole), 50 µL per slide (1 µg/mL).

Basically the same procedure was applied for the measurement of DNA base damage. The treated cells were incubated on slides with the formamido-pyrimidine DNA glycosylase (FPG, New England BioLabs, UK), as described in [24]. Briefly, after lysis, the slides were washed 3 × 5 min with the FPG buffer (40 mM Hepes (4-(2-hydroxyethyl)-1-piperazine ethanesulfonic acid), 0.1 M KCl, 0.5 mM EDTA, 0.2 mg/mL bovine serum albumin, pH 8) at 4 °C. Further, 50 µL of FPG solution (4.8×10^{-2} U) in the buffer was placed on each slide, covered with cover glass and incubated for 30 min in a light-protected box at 37 °C. The slides were stained with DAPI (1 µg/mL) and analysed as described above. Image analysis of the data was performed with the Comet Assay IV Image Analysis System (Perceptive Instruments, UK). Fifty randomly selected comets per slide were analysed, two slides per experimental point. The percentage of DNA in the comet tail was used in this study as a measure of DNA damage.

The induction of DNA damage by a combined treatment with AgNPs and DFO was compared to the "expected value". The "expected value" concept is based on the assumption that action of both factors (NPs and DFO) is independent, and their combined toxicity is a sum of toxicities of each factor alone (neutral effect). If the combined toxicity is lower than the "expected value", the sparring effect is observed. If the combined toxicity is higher than the "expected value", the synergistic (potentiating) effect is observed.

2.5. Detection of H$_2$O$_2$ in mitochondria

2.5.1. Cell transfection with Hyper Mito plasmid

pHyPer-dMito plasmid was purchased from Evrogen (Russia) To ensure that maximum transfection rate is achieved, the electroporation parameters have been optimized for HepG2 cells. Cells were harvested in the exponential growth phase, diluted in culture medium DMEM and the number of cells was determined using a Countess Automated Cell Counter (Invitrogen). One million HepG2 cells were span down and resuspended in 800 µL of Eppendorf Hypoosomal Electroporation Buffer. Ten micrograms of plasmid DNA were added and mixed well. Afterwards the cell suspension was transferred to 4 mm gap width electroporation cuvettes and electroporation was carried out using the Eppendorf Multiporator set to following parameters: 500 V, 3 pulses and 100 µs time constant at room temperature. After pulsing the cells were allowed to remain in the cuvettes for 5 min and then carefully transferred into 3 mL of fresh culture medium DMEM with 10% FBS and cultivated in 6-well culture plates at least 24 h.

2.5.2. Hydrogen peroxide generation analysis

The analysis of AgNPs-induced generation of H_2O_2 in HepG2 cells transfected with pHyPer-dMito plasmid was carried out using an LSRII flow cytometer (BD). Cells were incubated for 90, 120 or 150 min with 12.5, 25 and 50 μg/mL AgNPs, harvested, resuspended in DMEM with 10% FBS and change of fluorescence intensity was measured with a LSRII flow cytometer (BD) (BD) on FITC-channel (FL-1). Autofluorescence of pHyPer-dMito untransfected, but similarly treated cells was subtracted from each experimental point.

2.6. Detection of H_2O_2 in cytosol

Cells were incubated for 2 h with 50 μg/mL AgNPs and dihydrorhodamine 123 was added to the final concentration 5 μM for 1 h. Cells were then harvested, resuspended in DMEM with 10% FBS and change of fluorescence intensity was measured with a LSRII cytometer (BD) on FITC-channel (FL-1).

2.7. Detection of $O_2^{\cdot-}$ in mitochondria

Cells were incubated for 2 h with 50 μg/mL AgNPs and MitoSox Red probe was added to the final concentration 5 μM for 40 min. Then, cells were harvested, resuspended in DMEM with 10% FBS and change of fluorescence intensity was measured with a LSRII flow cytometer (BD) on PE-channel (FL-2).

2.8. Detection of $O_2^{\cdot-}$ in cytosol

Cells were incubated for 2 h with 50 μg/mL AgNPs and dihydroethidine were added to the final concentration 5 μM for 1 h. Then, cells were harvested, resuspended in DMEM with 10% FBS and change of fluorescence intensity was measured with a LSRII flow cytometer (BD) on PE-channel (FL-2).

2.9. Statistics

If not otherwise indicated, significance of the difference of means was evaluated by Student t-test for independent samples. The time and AgNPs concentration dependence of generation of H_2O_2 in mitochondria was analysed by two-way ANOVA. Interaction of cytotoxic effects of DFO and AgNPs was evaluated by combination index method [21].

3. Results and discussion

Many TEM microphotographs clearly show that AgNPs of various sizes and shapes accumulate in the mitochondria. Thus, it is plausible to assume that NPs could be the direct cause of mitochondrial damage and malfunction of respiratory chain resulting in the ROS generation and oxidative stress. However, the primary product of failing electron transport chain is $O_2^{\cdot-}$ [25]. Due to its low chemical reactivity, $O_2^{\cdot-}$ is rather unlikely to cause harmful effects triggered by the presence of NPs [26]. In addition, being negatively charged $O_2^{\cdot-}$ does not pass freely through cell membranes and must be either protonated or converted to another uncharged compounds, to leave the mitochondria and exert detrimental effects in cytoplasm or nucleus. This discrepancy hampers our understanding of the basis of NPs induced toxicity. We anticipated that $O_2^{\cdot-}$ generated by mitochondria is dismutated to H_2O_2, and then $^{\cdot}OH$ is produced as a result of an iron-driven Fenton reaction. To solve this enigma we designed a set of experiments focused on the effects of iron chelation on AgNPs toxicity. In this study we used spherical AgNPs particles of nominal size 20 nm. The hydrodynamic diameter of AgNPs in Williams medium supplemented with 10% FCS was 78.22 ± 2.3 nm, polydispersity index 0.286, zeta potential– 33.6 mV. A detailed characteristics of the AgNPs used in this study, including its aggregation in time in different culture media was already published [22]. However, ions released from NPs to culture medium are a confounding factor,
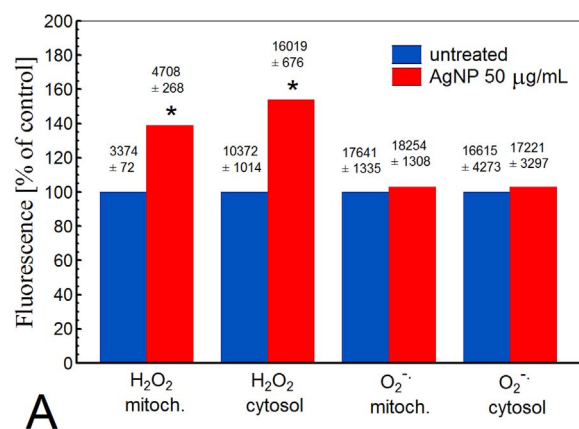

Fig. 1. ROS generation in HepG2 cells treated with 50 μg/mL of AgNPs. The level of H_2O_2 or $O_2^{\cdot-}$ in mitochondria or cytosol expressed as a percent of control value. AgNPs treatment induces production of hydrogen peroxide in cytosol and mitochondria, whereas the actual product of mitochondrial electron transport chain leakage, $O_2^{\cdot-}$, is not visible. The actual values of fluorescence are shown above the columns (mean ± SD, n = 3). Asterix (*) – mean statistically significant difference of mean from control, Student t-test, $P < 0.05$, df = 4.

when NPs toxicity is measured. Understanding the importance of this issue, we have previously measured AgNPs dissolution in experimental conditions similar to those used in this study. The results suggested only a negligible role of silver ions in our experimental design, even during long incubation times [19].

3.1. AgNPs-induced mitochondrial stress

Overproduction of ROS is proposed as a crucial mechanism for the toxicity of engineered NP, including AgNPs [10,11,13]. Thus, four different fluorescent probes were used to assess production of H_2O_2 and $O_2^{\cdot-}$ in mitochondria and cytoplasm of AgNPs-treated cells. HyPer-dMito indicator protein was used to estimate the mitochondrion specific production of H_2O_2. In cells treated with 50 μg/mL of AgNPs fluorescence from Hyper-Mito protein increased to 140% of the control level (Fig. 1). Further analysis of time- and concentration-dependence of AgNPs effects by two-way ANOVA revealed statistically important effect of AgNPs concentration ($P = 0.001$) and time ($P = 0.002$). Post-hoc analysis revealed a significant difference from the control (untreated) in cells after 120 and 150 min of treatment with 25 and 50 μg/mL AgNPs (Fig. 2). In contrast, measurements of mitochondrial $O_2^{\cdot-}$

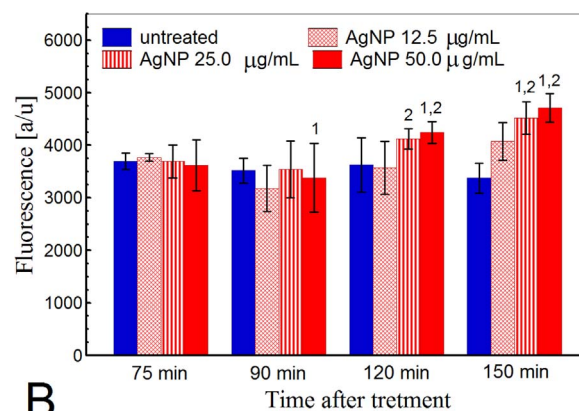**Fig. 2.** Time and concentration dependent generation of H_2O_2 in mitochondria in cells treated with 50 μg/mL of AgNPs (mean ± SD, n = 3). AgNPs treatment induces a time- and dose-dependent increase of generation of H_2O_2. 1 – denotes statistically significant difference of means from control (75 min, untreated); 2 – denotes statistically significant difference of means from the untreated and treated cells within the same time group, two-way ANOVA and post-hoc comparison by Fischer's LSD test, $P < 0.05$.

formation with MitoSox Red probe revealed only slight, if any, increase in $O_2^{\cdot-}$ formation. The increase in mitochondrial H_2O_2 production corresponded to the level of H_2O_2 in cytosol (150% of the control), as measured by dihydrorhodamine 123 assay. Also, in accordance with the mitochondrial $O_2^{\cdot-}$ production, no increase of $O_2^{\cdot-}$ level was observed in cytosol, as measured by dihydroethidine assay (Fig. 1).

While, NP dependent production of ROS is usually evaluated with fluorescent dyes of limited specificity, such as dichlorodihydro-fluorescein diacetate, that preclude exact determination of the nature of ROS produced, in this study we used a HyPer-dMito protein, the specificity of which was previously confirmed [27], leaving no doubts that H_2O_2 is produced by mitochondria of intact cells treated with AgNPs. Moreover, mitochondrial dysfunction and generation of H_2O_2 by mitochondria isolated from rats exposed to TiO_2NP was recently reported using a H_2O_2 specific dye – Amplex Red [28]. This is in agreement with a number of works on isolated mitochondria, in which production of H_2O_2 rather than $O_2^{\cdot-}$ was used as an indicator of mitochondria failure. It is thus believed that $O_2^{\cdot-}$ produced by a failing electron transport chain is dismutated by mitochondrial superoxide dismutase to H_2O_2 that can freely pass mitochondrial membranes. It is also in a good agreement with steady-state concentrations of $O_2^{\cdot-}$ (0.2–0.3 nM) and H_2O_2 (10–100 nM) in mitochondria [29].

3.2. Effect of DFO on AgNPs cytotoxicity

Nevertheless, production $O_2^{\cdot-}$ and/or H_2O_2 by mitochondria of NPs treated cells does not explain the observed nanoparticle geno- and cytotoxicity. Both compounds are not very reactive and rather unlikely to damage DNA or cause cell death. However, trace amounts of unprotected transition metal ions (Fe) can catalyse decomposition of H_2O_2 that gives rise to the highly reactive $^\cdot OH$, commonly accepted as the main source of oxidative damage to the cell [30]. Transition metal-driven generation of oxygen-derived free radicals is known to induce oxidation of proteins, lipids and lipoproteins, nucleic acids, carbohydrates and other cellular components. Indeed, pre-treatment with iron salts increased induction of DNA damage and decreased cell survival in vitro [31]. Studies on animals also revealed that iron overload caused an elevated level of DNA damage and lipid peroxidation [32]. Furthermore, a natural difference in CIP between two closely related L5178Y cell lines was claimed to be directly linked with cell susceptibility to H_2O_2 and DNA damage formation [33,34]. Also a positive correlation between CIP and the level of 8-oxo-7,8-dihydro-2˘-deoxyguanosine in DNA was reported in human lymphocytes, indicating a direct link between the unshielded iron and DNA damage [8].

On the other hand, CIP depletion by means of iron-specific chelators diminishes the deleterious effects of H_2O_2. The cell permeable iron chelator SIH, has been shown to protect cells from cyto- and genotoxic effects of H_2O_2, including mitochondrial injury [35]. Also, the cell non-permeable iron chelator, deferoxamine mesylate (DFO), has been shown to prevent detrimental effects of transition metal driven oxidative stress [23]. In the present work the effect of DFO on AgNPs-induced cytotoxicity was evaluated by NR assay in cells exposed to DFO for 2 h or 24 h prior to NP addition. DFO alone induced slight cytotoxicity in the tested cell line. In contrast, AgNPs showed marked, dose dependent cytotoxicity, reducing the number of living cells by 90% at a concentration of 100 µg/mL in the 48 h NR assay. However, pre-treatment of the cells for 2 h with DFO significantly increased the number of surviving cells, to about 20% at concentration of 100 µg/mL in the 48 h NR assay. As estimated from the additive effects of both compounds, no survivors should be observed in the 48 h NR assay among cells treated with 50 and 100 µg/mL AgNPs and DFO, whereas the actual surviving fraction were 30% and 20%, respectively (Fig. 3a). The analysis by combination index method [21] revealed moderate or strong antagonism of AgNPs and DFO at all simulated and actual doses (with the exception of dose combination: 25 µg/mL AgNPs and 2.5 µM DFO) (Fig. 4 and CompuSync report file AgNPs+DFO-d 2.pdf in

Supplementary materials).

Since DFO does not penetrate easily the cell membranes and is taken up predominantly by endocytosis/pinocytosis, it localizes almost exclusively within the lysosomal compartment [36]. Thus, the use of these two pre-exposure regimens allows for differentiation between the effects of chelation of endosomal/lysosomal iron (2 h pre-treatment) or the whole cell iron depletion (24 h pre-treatment). Our results indicate that the effects of 2 h pre-treatment with DFO do not differ substantially from that of 24 h pre-treatment (Fig. 3b), indicating a crucial role of lysosomal iron in NP-mediated toxic effects. This is in line with previously published data showing the crucial role of lysosomal iron in induction of DNA damage by extracellular H_2O_2 or ionizing radiation [37]. As the sites of intensive protein degradation, lysosomes and late-endosomes are believed to contain large amount of transition metal ions originating from digested metalloproteins. It was even suggested that lysosomes may contain a major pool of cellular red-ox active iron [38]. It was also shown that release and relocation of lysomal iron is an important mediator of oxidative-stress-induced DNA damage [39]. In this context NP can act a redox-active iron ions carrier. Binding metal ions is a natural property for many metal and non-metal NMs [40]. Iron contamination was shown to determine toxicity of multiwalled carbon nanotubes [41]. Since NPs are present in lysosomes [42,43], it is plausible to assume that unshielded iron ions in lysosomes bind the NPs, which are thereby transported to other cellular compartments, including mitochondria and nucleus. Alternatively, iron could be adsorbed on the AgNPs surface from culture medium when a primary protein corona is formed or it could remain as impurities after NP manufacture. However, in both cases availability of iron ions seems to be markedly lower than in lysosomes. Whether NPs-bound transition metal ions are still redox active is not known yet, but they can be readily released due to the NP's protein corona reorganization.

3.3. Effect of DFO on DNA damage induction by AgNPs

We have recently shown that formation of ROS and oxidative damage to DNA correlates well with a decrease in cell viability, measured by the ability of cell to form colonies after the AgNPs treatment [19]. Thus, induction of DNA damage by AgNPs in the presence of iron chelator, deferoxamine (DFO), was estimated using the comet assay. DFO alone did not induce DNA damage. In contrast, AgNPs treatment induced a significant increase in the percent of DNA in comet tail indicating induction of DNA damage. Both induction of single stand breaks (SSB), as measured by alkaline comet assay, and induction of oxidatively damaged DNA bases, as measured by FPG-glycosylase modified assay, were observed. Pre-treatment of AgNPs-exposed cells for 2 h with DFO caused a significant decrease in induction of DNA damage. In DFO pre-treated cells the level of AgNPs-induced SSB was similar to that of control, whereas in the case of oxidatively damaged DNA bases the reduction was approximately 50%, as compared to non-pre-treated cells. In both cases, DNA damage observed in pre-treated cells was significantly lower than expected from the additive action of both compounds (Fig. 5).

Though our results point to the importance of lysosomal iron in NP induced toxicity, mitochondria themselves, as a site of iron-sulphur cluster synthesis, have a high intrinsic concentration of chelatable iron [4,38]. Moreover $O_2^{\cdot-}$ was proven to oxidize the [4Fe–4S] clusters of dehydratases, such as aconitase, realising Fe^{+2} ions and further increasing the availability of iron for the Fenton reaction [44]. Whereas the actual origin of iron ions involved in NP-induced toxicity needs further investigations, our results leave no doubts that its chelation has a sparing effect and diminishes, both NP geno- and cytotoxicity.

g Altogether, our results strongly suggest that chelation of unshielded iron ions, in particular lysosomal iron, abolishes the toxic effect of AgNPs. This points to the crucial role of Fenton chemistry in oxidative-stress dependent NPs toxicity and solves the discrepancy between generation of relatively biologically inert compounds, such as
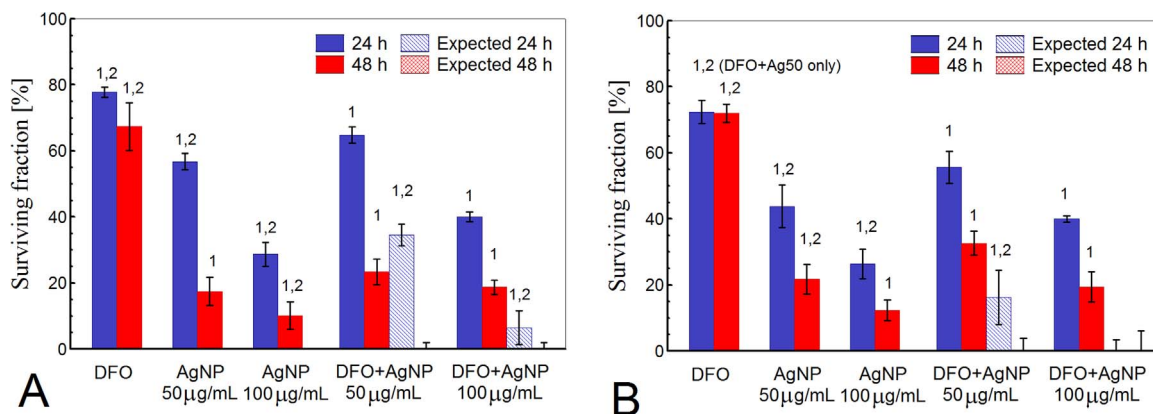
Fig. 3. Cytotoxicity of AgNPs in HepG2 cells pre-treated with DFO (25 μM). (a) 2 h pre-treatment. (b) 24 h pre-treatment, taking controls as 100%. Expected values reflect a sum of toxicity of AgNPs and DFO (additive effect). Whereas DFO induced only slight toxicity, treatment with AgNPs resulted in a marked decrease of cell survival. However, when cells were pre-treated with DFO, toxicity of AgNPs was significantly lower. 1 – denotes statistically significant difference of means from respective DFO + AgNPs treatment; 2 – denotes statistically significant difference of means between experimental and expected values. Mean ± SD, n = 4, Student *t*-test, $P < 0.05$, df = 6. Since some expected values were below zero, their significance was not evaluated. Statistical evaluation was performed on raw data presented in Supplementary Table 1.
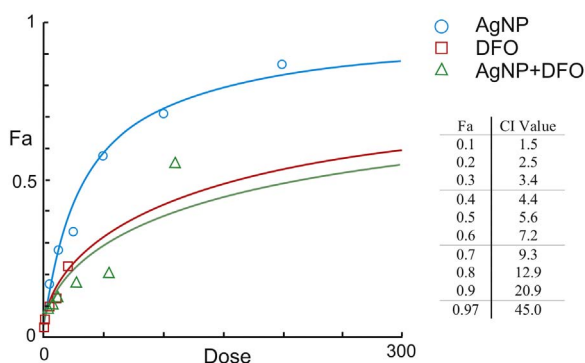

Fig. 4. Analysis of combined effect of AgNPs and DFO on survival of HepG2 cells according to combination index method [21]. Insert presents Combination index (CI) values for Drug Combo: Ag + DFO (Ag + DFO [10:1]), see CompuSync report file AgNPs + DFO-d 2.pdf (Supplementary materials) for full analysis. Fa – Fraction affected; CI values above 1 means antagonistic effect. A representative figure for 3 independent experiments. The analysis by combination index method clearly indicates that combined treatment with DFO and AgNPs in 1:10 ratio has strong sparring effect (antagonism) over a wide range of concentrations, as compared to the toxicity of AgNPs alone.
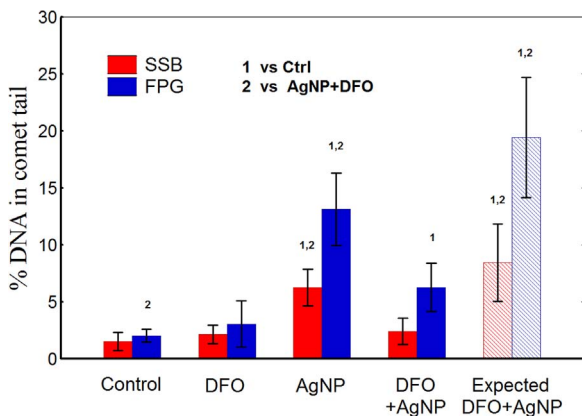

Fig. 5. Genotoxicity of AgNPs (10 μg/mL) in HepG2 cells pre-treated with DFO (100 μM) for 2 h. Expected values reflect a sum of genotoxicity of AgNPs and DFO. 1 – denotes statistically significant difference of means from control; 2 – denotes statistically significant difference of means from DFO + AgNPs treatment (mean ± SD, n = 4), Student *t*-test, $P < 0.05$, df = 6. Pretreatment with DFO has a sparing effect on AgNPs genotoxicity.
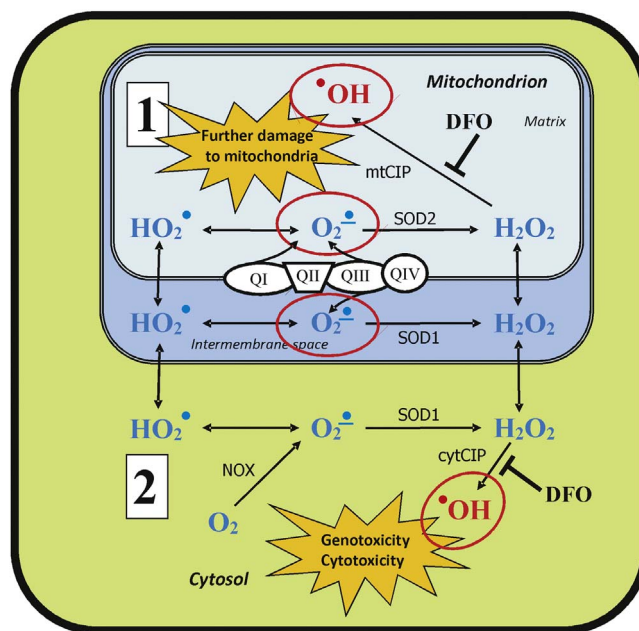

Fig. 6. A putative mechanism of induction of oxidative stress in AgNPs treated cells. [1] In mitochondrion. Superoxide anion radical ($O_2^{\bullet-}$) generated by leaking mitochondrial electron transport chain is either dismutated to hydrogen peroxide H_2O_2 by superoxide dismutase 2 (SOD2, in matrix) or superoxide dismutase 1 (SOD1, in intermembrane space), or protonated to form hydroperoxyl radical ($HO_2^{\bullet}$). Unlike $O_2^{\bullet-}$, $HO_2^{\bullet}$ and H_2O_2 easily cross cell membranes, and so can penetrate between mitochondrial compartments or to cytoplasm. H_2O_2 formed in the mitochondrion can migrate to cytoplasm or undergo iron-catalysed Fenton reaction to form very reactive hydroperoxyl radical ($^{\bullet}OH$). [2] In cytoplasm. $HO_2^{\bullet}$ can be deprotonated to form $O_2^{\bullet-}$, that is further dismutated to H_2O_2 by SOD1. $O_2^{\bullet-}$ is also generated by NADPH oxidase (NOX). H_2O_2 formed in cytoplasm can migrate to the mitochondrion or undergo iron-catalysed Fenton reaction to form very reactive $^{\bullet}OH$. QI-QIV – electron transport chain. mtCIP, cytCIP – mitochondrial or cytosoli chelatable iron pool. DFO – iron chelator, deferoxamine.

$O_2^{\bullet-}$ and/or H_2O_2, by NPs-exposed mitochondria and the detrimental effects of NPs predominantly dependent on highly active $^{\bullet}OH$ radical. A putative role of iron in AgNPs toxicity is summarized in Fig. 6. Whether this mechanism is universal for other types of NPs needs to be verified experimentally. However, having in mind the ubiquitous abundance of iron ions in living cells, the process seems to be prevalent as far as oxidative stress due to mitochondria dysfunction is concerned.

Acknowledgements

Author contributions

A.G. designed part of experiments, contributed in the data analysis and manuscript writing, M.W. made comet assay experiments, S.M-W. was responsible for cytotoxicity tests, M.Z. measured generation of H_2O_2 in mitochondria including pHyPer-dMito transfection, D.W. measured other ROS, M.K. designed study outline and part of experiments, analysed data and wrote the manuscript.

Competing financial interests

The authors declare no competing financial interests.

Appendix A. Supplementary material

Supplementary data associated with this article can be found in the online version at http://dx.doi.org/10.1016/j.redox.2018.01.006.

References

[1] K. Brzoska, S. Meczynska, M. Kruszewski, Iron-sulfur cluster proteins: electron transfer and beyond, Acta Biochim. Pol. 53 (4) (2006) 685–691.

[2] B. Halliwell, S. Chirico, Lipid peroxidation: its mechanism, measurement, and significance, Am. J. Clin. Nutr. 57 (1993) 715S–724S.

[3] E.S. Henle, S. Linn, Formation, prevention, and repair of DNA damage by iron/hydrogen peroxide, J. Biol. Chem. 272 (31) (1997) 19095–19098.

[4] M. Kruszewski, The role of labile iron pool in cardiovascular diseases, Acta Biochim. Pol. 51 (2) (2004) 471–480.

[5] F. Oliveira, S. Rocha, R. Fernandes, Iron metabolism: from health to disease, J. Clin. Lab. Anal. 28 (3) (2014) 210–218.

[6] A.C. Mello-Filho, R. Meneghini, Iron is the intracellular metal involved in the production of DNA damage by oxygen radicals, Mutat. Res. 251 (1) (1991) 109–113.

[7] M. Kruszewski, T. Iwanenko, Labile iron pool correlates with iron content in the nucleus and the formation of oxidative DNA damage in mouse lymphoma L5178Y cell lines, Acta Biochim. Pol. 50 (1) (2003) 211–215.

[8] D. Gackowski, M. Kruszewski, T. Bartlomiejczyk, A. Jawien, M. Ciecierski, R. Olinski, The level of 8-oxo-7,8-dihydro-2′-deoxyguanosine is positively correlated with the size of the labile iron pool in human lymphocytes, J. Biol. Inorg. Chem. 7 (4) (2002) 548–550.

[9] M. Kruszewski, Labile iron pool: the main determinant of cellular response to oxidative stress, Mutat. Res. 531 (1–2) (2003) 81–92.

[10] M. Kruszewski, K. Brzoska, G. Brunborg, N. Asare, M. Dobrzynska, M. Dusinská, L. Fjellsbř, A. Georgantzopoulou, J. Gromadzka-Ostrowska, A. Gutleb, A. Lankoff, Z. Magdolenová, E. Pran, A. Rinna, C. Instanes, J. Sandberg, P. Schwarze, T. Stepkowski, M. Wojewódzka, M. Refsnes, Toxicity of silver nanomaterials in higher eukaryotes, in: J.C. Fishbein (Ed.), Advances in Molecular Toxicology, Elsevier B.V., Oxford, Amsterdam, 2011, pp. 179–218.

[11] T. Bartlomiejczyk, A. Lankoff, M. Kruszewski, I. Szumiel, Silver nanoparticles – allies or adversaries? Ann. Agric. Environ. Med. 20 (1) (2013) 48–54.

[12] P.P. Fu, Q. Xia, H.M. Hwang, P.C. Ray, H. Yu, Mechanisms of nanotoxicity: generation of reactive oxygen species, J. Food Drug Anal. 22 (1) (2014) 64–75.

[13] Z. Magdolenova, A. Collins, A. Kumar, A. Dhawan, V. Stone, M. Dusinska, Mechanisms of genotoxicity. A review of in vitro and in vivo studies with engineered nanoparticles, Nanotoxicology 8 (3) (2014) 233–278.

[14] A. Rinna, Z. Magdolenova, A. Hudecova, M. Kruszewski, M. Refsnes, M. Dusinska, Effect of silver nanoparticles on mitogen-activated protein kinases activation: role of reactive oxygen species and implication in DNA damage, Mutagenesis 30 (1) (2015) 59–66.

[15] Y. Mo, R. Wan, S. Chien, D.J. Tollerud, Q. Zhang, Activation of endothelial cells after exposure to ambient ultrafine particles: the role of NADPH oxidase, Toxicol. Appl. Pharmacol. 236 (2) (2009) 183–193.

[16] P.H. Hemmerich, A.H. von Mikecz, Defining the subcellular interface of nanoparticles by live-cell imaging, PLoS One 8 (4) (2013) e62018.

[17] P.V. AshaRani, M.P. Hande, S. Valiyaveettil, Anti-proliferative activity of silver nanoparticles, BMC Cell Biol. 10 (2009) 65.

[18] S.M. Hussain, K.L. Hess, J.M. Gearhart, K.T. Geiss, J.J. Schlager, In vitro toxicity of nanoparticles in BRL 3A rat liver cells, Toxicol. Vitr. 19 (7) (2005) 975–983.

[19] M. Kruszewski, I. Gradzka, T. Bartlomiejczyk, J. Chwastowska, S. Sommer, A. Grzelak, M. Zuberek, A. Lankoff, M. Dusinska, M. Wojewodzka, Oxidative DNA damage corresponds to the long term survival of human cells treated with silver nanoparticles, Toxicol. Lett. 219 (2) (2013) 151–159.

[20] L.L. Maurer, J.N. Meyer, A systematic review of evidence for silver nanoparticle-induced mitochondrial toxicity, Environ. Sci.: Nano 3 (2) (2016) 311–322.

[21] N. Zhang, J.N. Fu, T.C. Chou, Synergistic combination of microtubule targeting anticancer fludelone with cytoprotective panaxytriol derived from Panax ginseng against MX-1 cells in vitro: experimental design and data analysis using the combination index method, Am. J. Cancer Res. 6 (1) (2016) 97–104.

[22] A. Lankoff, W.J. Sandberg, A. Wegierek-Ciuk, H. Lisowska, M. Refsnes, B. Sartowska, P.E. Schwarze, S. Meczynska-Wielgosz, M. Wojewodzka, M. Kruszewski, The effect of agglomeration state of silver and titanium dioxide nanoparticles on cellular response of HepG2, A549 and THP-1 cells, Toxicol. Lett. 208 (3) (2012) 197–213.

[23] M. Kruszewski, M.H. Green, J.E. Lowe, I. Szumiel, Comparison of effects of iron and calcium chelators on the response of L5178Y sublines to X-rays and H2O2, Mutat. Res. 326 (1995) 155–163.

[24] M. Kruszewski, T. Iwanenko, Induction of DNA breakage in X-irradiated nucleoids selectively stripped of nuclear proteins in two mouse lymphoma cell lines differing in radiosensitivity, Acta Biochim. Pol. 45 (3) (1998) 701–704.

[25] S. Drose, U. Brandt, Molecular mechanisms of superoxide production by the mitochondrial respiratory chain, Adv. Exp. Med. Biol. 748 (2012) 145–169.

[26] L. Benov, How superoxide radical damages the cell, Protoplasma 217 (1–3) (2001) 33–36.

[27] D.S. Bilan, V.V. Belousov, HyPer family probes: state of the art, Antioxid. Redox Signal. 24 (13) (2015) 731–751.

[28] P.A. Stapleton, C.E. Nichols, J. Yi, C.R. McBride, V.C. Minarchick, D.L. Shepherd, J.M. Hollander, T.R. Nurkiewicz, Microvascular and mitochondrial dysfunction in the female F1 generation after gestational TiO2 nanoparticle exposure, Nanotoxicology 9 (8) (2015) 941–951.

[29] E. Cadenas, A. Boveris, Mitochondrial free radical production, antioxidant defenses and cell signaling, in: T. Grune (Ed.), Oxidants and Antioxidant Defense Systems, Springer-Verlag, Berlin Heidelberg, 2005, pp. 219–234.

[30] S.I. Liochev, I. Fridovich, The relative importance of HO. and ONOO- in mediating the toxicity of O, Free Radic. Biol. Med. 26 (5–6) (1999) 777–778.

[31] V. Abalea, J. Cillard, M.P. Dubos, J.P. Anger, P. Cillard, I. Morel, Iron-induced oxidative DNA damage and its repair in primary rat hepatocyte culture, Carcinogenesis 19 (6) (1998) 1053–1059.

[32] M. Galleano, S. Puntarulo, Hepatic chemiluminescence and lipid peroxidation in mild iron overload, Toxicology 76 (1) (1992) 27–38.

[33] P. Lipinski, J.C. Drapier, L. Oliveira, H. Retmanska, B. Sochanowicz, M. Kruszewski, Intracellular iron status as a hallmark of mammalian cell susceptibility to oxidative stress: a study of L5178Y mouse lymphoma cell lines differentially sensitive to H2O2, Blood 95 (9) (2000) 2960–2966.

[34] T.H. Zastawny, M. Kruszewski, R. Olinski, Ionizing radiation and hydrogen peroxide induced oxidative DNA base damage in two L5178Y cell lines, Free Radic. Biol. Med. 24 (7–8) (1998) 1250–1255.

[35] T. Simunek, C. Boer, R.A. Bouwman, R. Vlasblom, A.M. Versteilen, M. Sterba, V. Gersl, R. Hrdina, P. Ponka, J.J. de Lange, W.J. Paulus, R.J. Musters, SIH-a novel lipophilic iron chelator–protects H9c2 cardiomyoblasts from oxidative stress-induced mitochondrial injury and cell death, J. Mol. Cell. Cardiol. 39 (2) (2005) 345–354.

[36] H. Cable, J.B. Lloyd, Cellular uptake and release of two contrasting iron chelators, J. Pharm. Pharmacol. 51 (2) (1999) 131–134.

[37] C. Berndt, T. Kurz, M. Selenius, A.P. Fernandes, M.R. Edgren, U.T. Brunk, Chelation of lysosomal iron protects against ionizing radiation, Biochem. J. 432 (2) (2010) 295–301.

[38] F. Petrat, H. de Groot, U. Rauen, Determination of the chelatable iron pool of single intact cells by laser scanning microscopy, Arch. Biochem. Biophys. 376 (1) (2000) 74–81.

[39] T. Kurz, A. Leake, T. von Zglinicki, U.T. Brunk, Lysosomal redox-active iron is important for oxidative stress-induced DNA damage, Ann. N. Y. Acad. Sci. 1019 (2004) 285–288.

[40] M. Hua, S. Zhang, B. Pan, W. Zhang, L. Lv, Q. Zhang, Heavy metal removal from water/wastewater by nanosized metal oxides: a review, J. Hazard. Mater. 211–212 (2012) 317–331.

[41] E. Aldieri, I. Fenoglio, F. Cesano, E. Gazzano, G. Gulino, D. Scarano, A. Attanasio, G. Mazzucco, D. Ghigo, B. Fubini, The role of iron impurities in the toxic effects exerted by short multiwalled carbon nanotubes (MWCNT) in murine alveolar macrophages, J. Toxicol. Environ. Health A 76 (18) (2013) 1056–1071.

[42] E. Frohlich, C. Meindl, E. Roblegg, B. Ebner, M. Absenger, T.R. Pieber, Action of polystyrene nanoparticles of different sizes on lysosomal function and integrity, Part. Fibre Toxicol. 9 (1) (2012) 1–13.

[43] L.J. Lucas, X.K. Chen, A.J. Smith, M. Korbelik, H. Zeng, P.W.K. Lee, K.C. Hewitt, Aggregation of nanoparticles in endosomes and lysosomes produces surface-enhanced Raman spectroscopy, J. Nanophoton. 9 (1) (2015) 093094.

[44] K. Keyer, J.A. Imlay, Superoxide accelerates DNA damage by elevating free-iron levels, Proc. Natl. Acad. Sci. USA 93 (24) (1996) 13635–13640.